

Molecular Orientation in Deformed Bimodal Networks. 2. Fourier Transform Infrared Measurements on Poly(dimethylsiloxane) Networks and Comparison with Theory

S. Besbes, L. Bokobza, and L. Monnerie

Laboratoire de Physico-Chimie Structurale et Macromoléculaire, ESPCI, 10 rue Vauquelin,
75231 Paris Cedex 05, France

I. Bahar* and B. Erman

Polymer Research Center and School of Engineering, Bogazici University, and TUBITAK
Advanced Polymeric Materials Research Center, Bebek 80815, Istanbul, Turkey

Received March 14, 1994; Revised Manuscript Received September 7, 1994[®]

ABSTRACT: Results of segmental orientation in uniaxially stretched bimodal poly(dimethylsiloxane) networks are reported. Measurements are carried out by Fourier transform infrared dichroism spectroscopy. Bimodal networks were formed by tetrafunctionally end-linking low molecular weight ($M_n = 5600$) deuterated chains with high molecular weight ($M_n = 20000$) hydrogenated chains. Independent measurements of segmental orientation of the short and the long chains showed that the short (long) ones orient less (more) than the corresponding chains of the unimodal networks, in conformity with the predictions of the theory developed in the preceding paper. Furthermore, the change in segmental orientation of short and/or long chains in bimodal networks relative to their unimodal counterparts, expressed by the ratios S_S/S_S° or S_L/S_L° , is in reasonable quantitative agreement with the theory. Experiments show that the orientations of the short and the long chains in bimodal networks are approximately equal to each other. On the other hand, the theory based on the phantom network model predicts that the long chains should orient less than the short ones. In fact, some departure between theory and experiments is observed in the case of longer chains, whose behavior does not conform with the phantom network model underlying the theory. The differences between theory and experiments are attributed to the effects of entanglements which operate to different extents for different chain lengths.

Introduction

Recent Fourier transform infrared measurements of Hanyu and Stein¹ and deuterium NMR measurements of Chapellier et al.² on segmental orientation in uniaxially stretched bimodal networks have shown that the orientations of the short and the long chains are approximately equal. Under the light of previous theoretical work, this result does not conform with earlier theoretical evidence by Higgs and Ball³ based on the phantom network model which indicates that the short chains should orient more than the long ones. In the interest of pursuing this subject further, we have performed a detailed theoretical investigation of segmental orientation as well as an experimental study. The theoretical work,⁴ constituting the first part of this study presented in the previous paper, has indicated, in agreement with the predictions of Higgs and Ball, that the short chains should orient more than the long ones in the bimodal network. The theory is based on the phantom network model whereas the real networks studied in the experiments, and the long chains in particular, depart to some extent from that model and are subject to the effects of entanglements. The contributions from entanglements⁵⁻⁹ might affect the deformations of the long and the short chains of the bimodal network to different extents, resulting in departures from the expected orientational behavior of phantom bimodal networks.

To check the predictions of the theory for bimodal networks,⁴ it is necessary to measure the molecular orientation of the long and the short chains independently. Among the techniques used to characterize

molecular orientation, infrared dichroism seems to be the most suitable for this purpose. By deuterating one type of the chains, the technique of Fourier transform infrared dichroism is able to measure the orientations of the two types of chains independently. This is possible effectively because of the mass dependence of the vibrational frequency, as a result of which pronounced frequency shifts result upon isotopic substitution.

In the following, we report results of Fourier transform infrared dichroism measurements performed on bimodal and unimodal poly(dimethylsiloxane) networks in which the short chains are deuterated and the long ones are hydrogenated. Results are compared with the predictions of the theory developed in the preceding paper. Departures between theory and experiments will be discussed by invoking the constraints from entanglements.

Experimental Section

The use of specific chemical reactions for the cross-linking process permits control of the network structure. End-linking polymer chains by means of a multifunctional cross-linking agent provides an ideal way for obtaining elastomeric networks of any desired distribution of chain lengths. Of specific interest are bimodal networks prepared in this study by end-linking hydrogenated long chains ($M_n = 20000$) and deuterated short chains ($M_n = 5600$), each having a polydispersity index of 2. Exact stoichiometric amounts of 1,3,5,7-tetravinyl-1,3,5,7-tetramethylcyclotetrasiloxane were used as a tetrafunctional cross-linking agent.⁷ The syntheses were performed in the bulk in the presence of chloroplatinic acid used as a catalyst. The reacting mixture was cast onto a Teflon plate, and the cross-linking reaction was carried out there at 80 °C for 5-10 h. Three different samples with weight fractions of short chains $w = 0.26, 0.34, \text{ and } 0.53$, denoted respectively B-1, B-2, and B-3, were prepared. Unimodal networks of long (U-L) and short (U-S) chains were also prepared (See Table 1).

[®] Abstract published in *Advance ACS Abstracts*, November 1, 1994.

Table 1. Characteristics of the Networks Used in the Experiments

sample ^a	wt fraction of short chains, w
U-L	0.0
U-S	1.0
B-1	0.26
B-2	0.34
B-3	0.53

^a M_n of long chains in both the unimodal and bimodal networks = 20000; M_n of short chains in both the unimodal and bimodal networks = 5600.

The specimens (8 mm × 35 mm × 0.2 mm) were stretched with a manual stretching machine that allows symmetrical uniaxial deformation, and infrared spectra were obtained with a Fourier transform infrared Nicolet 7199 spectrometer, using a resolution of 2 cm⁻¹ and 100 scans.

Segmental orientation S in a network submitted to uniaxial elongation may be conveniently described by the second Legendre polynomial $S = \frac{1}{2}(3 \cos^2 \theta - 1)$, where θ is the angle between the direction of extension and the local chain axis of the polymer. The dichroic ratio R , defined as $R = a_{\parallel}/a_{\perp}$ (a_{\parallel} and a_{\perp} being the absorbances of the investigated band, measured with radiation polarized parallel and perpendicular to the stretching direction, respectively), is the parameter commonly used to characterize the degree of optical anisotropy in stretched polymers. S is related to the dichroic ratio R by the expression

$$S = [2/(3 \cos^2 \alpha - 1)][(R - 1)/(R + 2)] \quad (1)$$

where α is the angle between the transition moment vector of the vibrational mode considered and the local chain axis of the polymer or any directional vector characteristic of a given chain segment.

For the hydrogenated chains, we have investigated the band at 2500 cm⁻¹, ascribed to the overtone of the symmetrical bending vibration. The orientation of the short deuterated chains was determined through the dichroic behavior of the band at 2126 cm⁻¹, which was attributed to the symmetrical stretching mode of the deuterated methyl groups. The transition moment associated with both vibrational modes lies along the CH₃-Si (or CD₃-Si) bond, which is a symmetry axis of the methyl group. The angle α between this transition moment and the segment joining two successive oxygen atoms chosen as the directional vector thus equates to 90°. A more detailed description of the technique and its application to poly(dimethylsiloxane) networks is given in previous work.^{7,8}

Experimental Results

The dependence of the orientation function S on the deformation term ($\lambda^2 - \lambda^{-1}$) is presented in Figure 1 for the bimodal network with $w = 0.26$. Here, λ denotes the extension ratio, defined as the ratio of the final length of the sample to that in the undeformed state. The open triangles and circles represent the experimental data for the networks U-S and U-L, respectively.

The experimental data for short and long chains in bimodal networks are shown by the filled triangles and circles, respectively. The upper curve represents the best fitting line for segmental orientation in the unimodal network of short chains, and the lower curve represents that for the unimodal network of long chains. The middle two curves represent the segmental orientation of the short and the long chains of the bimodal network. Similar graphs are presented in Figures 2 and 3 for networks with $w = 0.34$ and 0.53 , respectively. The scatter in the data points is intrinsic to the optical technique. Effectively, one of the problems in the standard way of measuring linear infrared dichroism is the lack of sensitivity in the determination of small

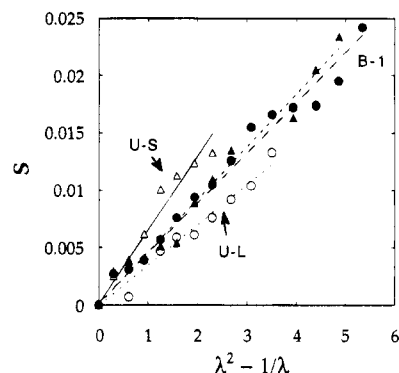


Figure 1. Dependence of the orientation function on the deformation term ($\lambda^2 - \lambda^{-1}$) for the two unimodal networks U-L and U-S as well as those of the long and short chain segments of the bimodal network B-1. The solid straight line is the best fitting line through the data points (open triangles) of U-S, and the dotted line is that through the data points (open circles) of U-L. The short dashed line goes through data points (filled triangles) for the short chains of B-1, and the long dashed line goes through the data points (filled circles) for the long chains of B-1.

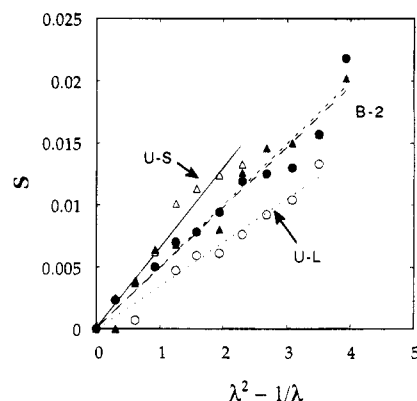


Figure 2. Dependence of the orientation function on the deformation term ($\lambda^2 - \lambda^{-1}$) for the two unimodal networks U-L and U-S as well as those of the long and short chain segments of the bimodal network B-2. (See legend for Figure 1.)

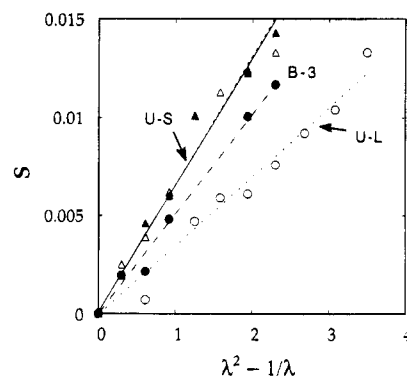


Figure 3. Dependence of the orientation function on the deformation term ($\lambda^2 - \lambda^{-1}$) for the two unimodal networks U-L and U-S as well as those of the long and short chain segments of the bimodal network B-3. (See legend for Figure 1.)

dichroic effects. This is the case for films under low deformation or in the polymers exhibiting slight orientations, which is exactly the case for the PDMS chains. In this case, the magnitude of $\Delta a = (a_{\parallel} - a_{\perp})$ is small and $R = a_{\parallel}/a_{\perp}$ is close to unity. On the other hand, the standard dichroism measurements require two different spectra of the sample to get the polarized absorptions

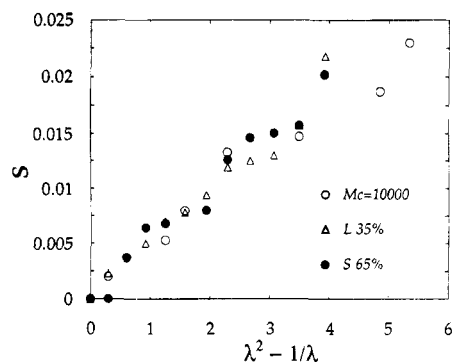


Figure 4. Comparison of the orientation functions of the long and short chain segments in the B-2 bimodal network with those of a unimodal network of $M_c = 10000$. Open triangles and filled circles represent data points for the long and short chains of B-2, respectively. Open circles are for the unimodal network.

parallel and perpendicular to the stretching direction in order to form either the dichroic ratio R or the dichroic difference $\Delta\alpha$. Some errors can be generated by repositioning the sample or the polarizer for the second measurement. At the present time, for samples where the dichroic ratio is nearly unity, only a polarization-modulation approach can yield measurements of small dichroic effects with a very high sensitivity. This technique allows a direct evaluation of the dichroic difference $\Delta\alpha$ in a single measurement. Moreover, it obviates the need for rotating either the sample or the polarizer when recording dichroic spectra.

It can be seen from Figures 1–3 that the segmental orientations of short and long chains of the two bimodal networks with $w = 0.26$ and 0.34 differ from those of the unimodal networks. In these two samples, the segmental orientation of the short (long) chains of the bimodal network is less (more) than that of the short (long) chains of the unimodal network. In the third bimodal network with $w = 0.53$, the orientation of short chains approximately equals that of the unimodal network U-S, while the long chains orient more than the chains of the corresponding unimodal network.

In the first bimodal network (Figure 1) containing nearly the same number of long and short chains, the orientations of the two types of chains are approximately equal. A similar conclusion can be drawn for the network containing a higher content of short chains (Figure 2). In the third network with $w = 0.53$, the orientation of the short chains is higher than that of the long chains. Our experimental results differ, in part, from those obtained by Hanyu and Stein¹ on model bimodal networks of poly(tetrahydrofuran) where the short and long chains exhibit equal segmental orientation irrespective of network composition.

The equality of the orientation functions led Hanyu and Stein¹ to the suggestion that the long and short chain segments are not equally strained at the molecular level. Following the work of Hanyu and Stein, results of segmental orientation measurements of the short and the long chains of the bimodal network with $w = 0.34$ are compared in Figure 4 with the results of measurements on a uniaxial network of molecular weight of 10000, which is equal to the average molecular weight of the bimodal network. Close agreement of the two results suggests the possibility of estimating segmental orientation of bimodal networks from unimodal networks of an equivalent molecular weight. The results are not conclusive, however, and more thorough experiments are needed.

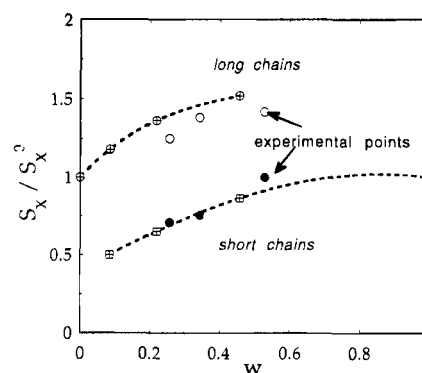


Figure 5. Ratio S_X/S_X^0 of segmental orientation of short ($X = S$) or long ($X = L$) chains in bimodal networks compared to those in unimodal networks as a function of weight fraction of short chains. The empty and filled circles represent experimental data for long and short chains, respectively. Symbols with a “+” sign and the dashed curves represent the corresponding theoretical results based on eqs 35 and 36 of the preceding paper.

Our results reveal the occurrence of somewhat distinct orientations in the two components of the network only when the network has a high content of short chains. By increasing the amount of short chains, an enhancement in the orientation of the long chains is observed while the short chains become less and less sensitive to the presence of long chains. Static¹⁰ and dynamic¹¹ light scattering studies performed on bimodal PDMS networks suggest heterogeneous structures with small mesh domains formed by many short chains instead of a homogeneous structure where long and short chains are randomly end-linked to each other. The formation of such heterogeneous structures could be due to a higher probability of end-linking of short chains than that of the long chains. Despite these considerations on heterogeneous systems, it is interesting now to compare our experimental results with the theoretical approach based on the model of the regular bimodal phantom networks developed in the preceding paper.

Comparison with Theory and Discussion

Figure 5 displays the ratio of the segmental orientation in bimodal networks to that observed in unimodal networks as a function of weight fraction of short chains. These ratios are denoted S_S/S_S^0 for short chains and S_L/S_L^0 for long chains. The empty circles represent measurements of orientation of the long chains, and the filled circles are for the short chains. The dashed curves are obtained from eqs 35 and 36 of the preceding paper using the experimental value of $\xi = 5600/20000 = 0.28$. According to the theoretical model of regular tetrafunctional bimodal networks, the composition may take only three values of mole fraction of short chains: 0.25, 0.50, and 0.75 for S_1L_3 , S_2L_2 , and S_3L_1 , respectively. These values correspond to the weight fractions $w = 0.085$, 0.22, and 0.45 when the molecular weights of the short and long chains are taken as 5600 and 20000, respectively. The points obtained by the theory on the two curves of Figure 5 are shown by the squares and circles filled with “+” sign. In addition to the three values of w for the bimodal networks, the points corresponding to the unimodal network are also shown on each curve.

It is to be noted that the theoretical curves of Figure 5 are obtained for a phantom network whereas the experimental data correspond to real networks. Despite

this difference, a fairly good agreement is obtained between the experimental data and theory. In the interest of establishing a connection between real networks and the theory presented in the preceding paper,⁴ we base our subsequent theoretical interpretation on the approximation

$$\frac{S_X}{S_X^\circ} = \frac{S_{X,\text{ph}}}{S_{X,\text{ph}}^\circ} \quad (2)$$

which is suggested by the experimental results displayed in Figure 5. Here, X is either L or S and the superscript "°" denotes the unimodal network. Writing eq 2 separately for L and S and taking ratios lead to the following expression:

$$\frac{S_L}{S_S} = \left(\frac{S_{L,\text{ph}}/S_{L,\text{ph}}^\circ}{S_{S,\text{ph}}/S_{S,\text{ph}}^\circ} \right) \frac{S_L^\circ}{S_S^\circ} \quad (3)$$

The terms in parentheses are given by eqs 35 and 36 of the preceding paper. The ratio S_L°/S_S° on the right-hand side refers to the orientations of real unimodal networks with long and short chains.

Equation 3 allows for the calculation of the ratio S_L/S_S for real bimodal networks in terms of the orientations of the bimodal phantom networks, calculated by the theory, and the ratio S_L°/S_S° of real unimodal networks. Segmental orientation in unimodal networks has been studied extensively, both theoretically and experimentally. Comparison of experimental data on unimodal networks with various theoretical expressions has shown that the essential features of the phenomena may satisfactorily be presented by adopting the constrained junction model⁵ of rubber elasticity. Here, we adopt this model in expressing the ratio S_L°/S_S° that appears in eq 3. According to the constrained junction theory,⁵ the orientation for the unimodal network is

$$S_X^\circ = \left(1 - \frac{2}{\phi}\right) D_X^\circ \left[\lambda^2 - \lambda^{-1} + \frac{2}{\phi - 2} (B_{1X} - B_{2X}) \right] \quad (4)$$

Here, ϕ is the junction functionality and D_X° is the configurational front factor for the unimodal network chains of type X. D_X° is inversely proportional to the molecular weight M_c of a network chain between crosslinks. An additional term in eq 4 which has been attributed to the deformation of constraint domains has been omitted^{5,12,13} in this first approximation. The function B_{iX} is given as

$$B_{iX} = \kappa_X^2 (\lambda_i^2 - 1) / (\kappa_X + \lambda_i^2)^2 \quad (5)$$

Here, $i = 1$ for the direction of stretch and 2 for the lateral direction. Accordingly, $\lambda_1 = \lambda$, and $\lambda_2 = 1/\lambda^{1/2}$. κ_X is the interpenetration parameter of the constrained junction model for the unimodal network of species X. According to the theory,¹⁵ κ scales with $M_c^{1/2}$. In the extreme limit of networks with very large M_c , κ becomes infinitely large. In this limit, the behavior of the network is close to that of the affine model. In the opposite extreme of networks with very small M_c , the value of κ approaches zero and the behavior of the network is close to that of the phantom network model. According to this discussion, one expects κ_L to be larger than κ_S .

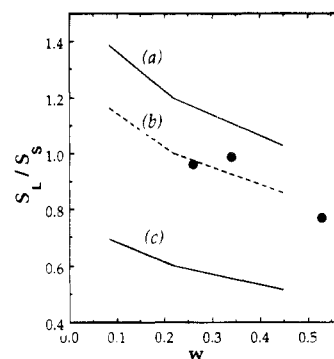


Figure 6. Ratio of the orientation of long chains to that of short chains. The filled circles represent experimental data. The curves are calculated from the theory. The phantom network model is adopted for short chains; accordingly, κ_S is taken as zero. For the long chains three cases corresponding to (a) the affine network model ($\kappa_L = \infty$), (b) the intermediate constrained junction model with $\kappa_L = 15$, and (c) the phantom network model ($\kappa_L = 0$) are shown.

Substituting eqs 35 and 36 of the preceding paper into eq 3 and using eq 4 lead to the following expression:

$$\frac{S_L}{S_S} = \frac{(A - 1)(B\xi + 1) D_L^\circ (\phi/2 - 1)(\lambda^2 - \lambda^{-1}) + B_{1L} - B_{2L}}{(A + 1)(B\xi - 1) D_S^\circ (\phi/2 - 1)(\lambda^2 - \lambda^{-1}) + B_{1S} - B_{2S}} \quad (6)$$

Results of experiments are compared with results of calculations based on eq 6 in Figure 6. The ordinate represents the ratio of the orientations in the long chains to that in the short ones for the bimodal network, and the abscissa is the weight fraction of short chains. The circles denote experimental results and the curves are from the theory. Like the results of Hanyu and Stein¹ and Chapellier et al.,² the experimental points indicate, approximately, equal orientations in the long and the short chains of the bimodal networks studied, although there is a slight decrease in the ratio with increasing w . As stated above, calculations are performed for the regular tetrafunctional bimodal network only at three values of w (0.085, 0.22, and 0.45). The curves shown in Figure 6 are obtained by calculating the ratio S_L/S_S at these values of w and connecting them by straight lines. In previous experiments, the segmental orientation in unimodal network chains of molecular weight 5600 was observed to conform closely with the predictions of the phantom network model. Accordingly, κ_S is taken as zero in the present calculations. For the long chains three cases corresponding to (a) the affine network model ($\kappa_L = \infty$), (b) the intermediate constrained junction model ($0 < \kappa_L < \infty$), and (c) the phantom network model ($\kappa_L = 0$) have been considered. These three cases are indicated by the labels (a), (b), and (c) appended to the curves. The upper curve may have a close connection to reality if the bimodal networks have extremely long and extremely short chains, resulting in affine-like behavior for the long chains and to phantom-like behavior for the short ones.^{14,15} In this sense, the two solid curves form the upper and the lower bounds for S_L/S_S . The dashed curve is calculated for exploratory purposes to see how close one may get to the experimental data by modifying the interpenetration parameter. The value of $\kappa_L = 15$ has been used in curve b. The curve calculated in this manner approximates the experimental data points satisfactorily.

As a concluding remark, we would like to point out that our interpretation of segmental orientation disagrees with that of Chapellier et al.² According to their model, segmental orientation results predominantly from intermolecular orientational coupling between neighboring segments. These segment-segment couplings are attributed to local steric effects. Our model is based on intramolecular effects rather than intermolecular effects, which is widely supported by experimental evidence.⁵⁻⁸ In fact, experiments on unimodal networks unequivocally show that segmental orientation is well described by the expression $S = D_0(\lambda^2 - \lambda^{-1})$. This equation is derived on the assumption that the network chains may take all possible configurations when their ends are fixed at separations consistent with the macroscopic strain. The front factor D_0 contains contributions from *intramolecular* effects only and varies inversely with chain length. Contributions from intermolecular effects to segmental orientation are observed to be negligible in swollen PDMS networks.⁸ D_0 might be written in the presence of intermolecular contributions as $D = D_0 + D_{\text{int}}$. Experiments show that D_{int} is approximately zero for PDMS networks. Therefore, we conclude that segmental orientation in bimodal PDMS networks predominantly reflects intramolecular contributions resulting from network topology, the

effects of bimodality, the constraints affecting junction fluctuations, and the state of macroscopic strain.

Acknowledgment. Partial support from Bogazici University Research Funds Project 94P0018 is gratefully acknowledged.

References and Notes

- (1) Hanyu, A.; Stein, R. S. *Makromol. Chem., Macromol. Symp.* **1991**, *45*, 189.
- (2) Chapellier, B.; Deloche, B.; Oeser, R. *J. Phys. II Fr.* **1993**, *3*, 1619.
- (3) Higgs, P. G.; Ball, R. C. *J. Phys. (Paris)* **1988**, *49*, 1785.
- (4) Bahar, I.; Erman, B.; Bokobza, L.; Monnerie, L. *Macromolecules* **1995**, *28*, 225.
- (5) Erman, B.; Monnerie, L. *Macromolecules* **1985**, *18*, 1985.
- (6) Mark, J. E.; Erman, B. *Rubberlike Elasticity: A Molecular Primer*; Wiley-Interscience: New York, 1988; p 196.
- (7) Besbes, S.; Cermelli, I.; Bokobza, L.; Monnerie, L.; Bahar, I.; Erman, B.; Herz, J. *Macromolecules* **1992**, *25*, 1949.
- (8) Besbes, S.; Bokobza, L.; Monnerie, L.; Bahar, I.; Erman, B. *Polymer* **1993**, *34*, 1179.
- (9) Erman, B.; Bahar, I.; Besbes, S.; Bokobza, L.; Monnerie, L. *Polymer* **1993**, *34*, 1858.
- (10) Soni, V. K.; Stein, R. S. *Macromolecules* **1990**, *23*, 5257.
- (11) Oikawa, H. *Polymer* **1992**, *33*, 1116.
- (12) Erman, B.; Flory, P. J. *Macromolecules* **1983**, *16*, 1601.
- (13) Erman, B.; Flory, P. J. *Macromolecules* **1983**, *16*, 1607.
- (14) Flory, P. J.; Erman, B. *Macromolecules* **1982**, *15*, 800.
- (15) Erman, B.; Flory, P. J. *Macromolecules* **1982**, *15*, 806.